Irrigation Science (2023) 41:197–214
https://doi.org/10.1007/s00271-023-00848-9

ORIGINAL PAPER

Remote sensing-based energy balance for lettuce in an arid environment: influence of management scenarios on irrigation and evapotranspiration modeling

Ramesh Dhungel[1] · Ray G. Anderson[1,2] · Andrew N. French[3] · Todd H. Skaggs[1] · Mazin Saber[4] · Charles A. Sanchez[5] · Elia Scudiero[1,2]

Received: 11 August 2022 / Accepted: 12 January 2023 / Published online: 24 January 2023

Abstract

Efficient irrigation is critical for managing scarce water resources where precipitation is minimal. Field-scale irrigation is largely unaccounted for in landscape evapotranspiration models, primarily due to the unavailability of data and the lack of water balance components in energy balance-based evapotranspiration models. To overcome these challenges, we implemented a remote sensing-based energy and water balance model BAITSSS (Backward-Averaged Iterative Two-Source Surface temperature Solution) to calculate evapotranspiration (ET) and irrigation requirements of winter lettuce in the arid environment of the Lower Colorado River Basin. Predicted evapotranspiration and irrigation were compared against data from twelve eddy covariance (EC) sites for wide range of soil hydraulic properties operating between 2016 and 2020 and the applied irrigation, respectively. BAITSSS estimated evapotranspiration and irrigation based on vegetative formation, weather demand, soil hydraulic characteristics, and predefined management allowed depletion (MAD) (0.4–0.6). Ground-based weather data, Sentinel-2-based vegetation indices, and SSURGO (NRCS soil survey database) soil moisture characteristics were model inputs. The results showed mean seasonal ET from BAITSSS and EC were comparable, differing on average by about 7% based on a constant rooting depth (500 mm) and MAD of 0.5 for entire crop growth stages. Variations in daily and seasonal ET were mainly due to differences in applied and model-simulated irrigation. Seasonal values of applied and simulated irrigation closely agreed (~6%) in most sites, though some sites applied irrigation more effectively than others. Overall, this study provided insight into consumptive water use and field-scale irrigation practices, as well as the capabilities and limitations of model-simulated ET and irrigation.

Introduction

Remote sensing-based energy balance models are frequently utilized to quantify crop water use (evapotranspiration) for water management (Allen et al. 2005; Anderson et al. 2012). To manage agricultural water, water managers compare evapotranspiration (ET) to applied water (groundwater pumping and irrigation diversions) (Allen et al. 2005). Field-scale irrigation practices (applied water) depend on multiple factors including farmers' experience, behavior, adaptability, investment in infrastructure, availability of water resources, and many others (Leng et al. 2017; de Vito et al. 2017; Foster et al. 2019). Landscape irrigation mapping needs information regarding land management (where and when humans have provided water or supplemented rain-fed crops) (Ozdogan et al. 2010). Accounting for field-scale irrigation in remote sensing-based landscape evapotranspiration (ET) maps is challenging due to inadequate spatial and temporal

✉ Ramesh Dhungel
ramesh.dhungel@usda.gov

1 USDA-Agricultural Research Service (ARS), US Salinity Laboratory, Agricultural Water Efficiency, and Salinity Research Unit, Riverside, CA 92507, USA

2 Department of Environmental Sciences, University of California, Riverside, 900 University Ave., Riverside, CA 92521, USA

3 USDA-ARS, US Arid Land Agricultural Research Center, 21881 N. Cardon Ln, Maricopa, AZ 85138, USA

4 University of Arizona, Yuma Agricultural Center, 6425 W 8th St, Yuma, AZ 85364, USA

5 University of Arizona, Maricopa Agricultural Center, 37860 W Smith Enke Rd, Maricopa, AZ 85138, USA

resolution (Ha et al. 2013). Irrigation alters soil moisture, and high spatial and temporal-resolution soil moisture maps can capture this critical piece of information related to the applied irrigation timing and amount. However, currently available soil moisture maps are mostly coarser resolution (> 25 km) (Brocca et al. 2017; Peng et al. 2021) and often provide information only about the upper soil moisture layer, for instance, microwave (~ 50 mm) (Kerr 2007; Collow et al. 2012; Ye et al. 2015; Akbar et al. 2018; Massari et al. 2021; Peng et al. 2021). Thus, these maps are generally useless where higher spatial resolution information is needed (Fang et al. 2019).

Thermal-based ET models often do not utilize irrigation directly in their surface energy balance algorithm, whereas the soil water balance-based ET models need information regarding irrigation and precipitation. However, the BAITSSS (Backward-Averaged Iterative Two-Source Surface temperature and energy balance Solution) (Dhungel et al. 2016, 2019) model accommodates water balance components in the energy balance algorithm and is used in operational settings (Dhungel et al. 2020). As field-scale irrigation information is not generally available, auto-irrigation in BAITSSS is based on weather demand, canopy formation (vegetation indices and physical properties), soil moisture characteristics, and predefined manageable allowed depletion (MAD). The estimated ET from BAITSSS represents the crop water requirements based on the irrigation management practice that should generally correspond to the applied irrigation in the field. However, discrepancies may arise due to the limitations in capturing the farmer's irrigation practices. Thus, a robust sensitivity analysis is needed to implement this model for regional irrigation scheduling and analysis effectively.

Previously, detailed evaluations of ET estimated with BAITSSS were conducted using eddy covariance (EC) data from 12 lettuce fields in the Lower Colorado River Basin (Dhungel et al. 2022), and using lysimeter ET data for corn and sorghum fields in Bushland, Texas (Dhungel et al. 2021). Both studies used the applied irrigation data as a model input, and the predicted ET closely agreed with both lysimeter and EC. In addition, the results showed the increased accuracy in ET estimation was due to the availability of applied irrigation in the field that was critical to capturing ET spikes right after the irrigation and tracking the continued decrease of ET after irrigation, especially during the partial cover period.

We extended the previous work focusing on lettuce in the Lower Colorado River Basin at the same sites and years (2016–2020). However, in this work, model calculations are made assuming the applied irrigation amounts, and timings are unknown. Irrigation scheduling in this region is commonly done based on the farmers'/producers' experience, rather than tracking soil moisture using field-based sensors or using specific computer-based irrigation simulation models. Farmers tend to well water and not stress crops due to the severe yield consequences of depleting short-season vegetable crops with shallow root zones (Kuslu et al. 2008; Xu and Leskovar 2014). To avoid water-related stress in most crop models, a management allowable depletion (MAD) of 0.5 is generally adopted (Clark 2000; Callison 2012; Malik and Dechmi 2019). However, this rough guideline is largely based on major grain/cereal crops; the sensitivity of vegetable crops is less known and may have lower permissible MAD (Hartz 1996; Thompson et al. 2007). General characteristics of ET simulation in winter vegetables including lettuce are shallow root depth compared to grain crops, short growing seasons, and longer partial cover period (Thorup-Kristensen 2001; Escarabajal-Henarejos et al. 2015; Roux et al. 2016; Fisher et al. 2017).

The overall objective of this study was to compare ET from eddy covariance (EC) with ET estimated from BAITSSS using auto-irrigation based on multiple predefined MAD's (0.4–0.6) (Allen et al. 1998; Bartlett et al. 2015). Irrigation and subsequent ET were estimated from the widely recommended MAD procedure suggested by university extension (Aguilar et al. 2015; Peters et al. 2013) which had not been fully investigated in landscape-scale remote sensing energy balance algorithm previously because of the aforementioned limitations.

Methodology

Study area

The study area comprised about 600 km^2 in commercially managed lettuce fields around Yuma, Arizona in the Lower Colorado River Basin. The Colorado River serves as the primary water source as precipitation is minimal (~ 80 mm/year) (Arguez et al. 2012). Sprinkler and furrow irrigation were used within the same season, with sprinkler irrigation used to help establish a crop and furrow irrigation used for the remainder of the season. Evapotranspiration estimated from BAITSSS was compared to twelve EC sites between 2016 and 2020. These sites were NGIDD 19–20a, YID 18b, YCWUA 18a, YID 17a, YID 19–20a, YCWUA 19–20a, YID 17d, YID 17b, YID 17c, YCWUA 17–18b, YCWUA 17–18a, and YID 16. NGIDDD represents North Gila Valley Irrigation and Drainage District, YID represents Yuma Irrigation District, and YCWUA represents Yuma County Water Users' Association. These lettuce fields were mostly rectangular shapes with a minimum and maximum area of 29,630 m^2 (YID19–20a) and 136,290 m^2 (YCWUA19–20a), respectively with an average of 105,699 m^2. Planting dates varied between September and November.

System components included three-dimensional sonic anemometers (CSAT3 and CSAT3A, Campbell Scientific, Logan, UT), open path infrared gas analyzers (IRGASON-Campbell Scientific and Licor 7500—Licor Inc., Lincoln, NE), net radiometers (NR-Lite and CNR 4, Kipp and Zonen, Delft, Netherlands), soil heat flux plates (Hukseflux, Delft, Netherlands), and air temperature and humidity probes (Vaisala, Helsinki, Finland). Loggers and covariance sensors were calibrated by the manufacturer in 2016 and 2017. Zero and span of infrared gas analyzers (IRGA) were done in July 2017 and again in July 2018.

Micrometeorological observations (~ 108 variables per 30 min. time step), configured under Campbell Scientific's EasyFlux DL™ (Logan, UT) program,[1] were collected to allow continuous data measurements during the cropping cycle. High-frequency three-dimensional wind, sonic temperature, and CO_2 and H_2O raw observations were collected at 20 Hz. A 30-min block-averaged fluxes, including the Webb–Pearman–Leuning (Webb et al. 1980) corrections were simultaneously stored and raw data were processed with EddyPro software in Express Mode (Fratini and Mauder 2014). We computed the changes in energy storage within the soil mass above the two heat flux plates. We removed the data spike followed the outlined methodology described by Vickers and Mahrt (1997). The online gap-filling tool (http://www.bgc-jena.mpg.de/~MDIwork/eddyproc/method.php); employing techniques as described in Falge et al. (2001) and Reichstein et al. (2005) were used to fill time gaps including those when the friction velocity (U^*) was less than 0.15 m/s. We conducted energy balance closure at daily time steps by regressing turbulent energy (latent heat and sensible heat) against radiative energy (net radiation minus ground heat flux) and correcting for net energy storage via photosynthesis (Anderson and Wang 2014). We enforced energy balance closure at 30-min time steps by assigning residuals to latent heat (LE) fluxes (Rosa and Tanny 2015). We conducted two-dimensional flux footprint analyses using an R script provided by Kljun et al. (2015). Eighty percent of the flux footprints lay within plot boundaries with minor exceptions where daily fluxes were computed by summing the 30-min LE flux values. Further details of EC data and processing can be found in French et al. (in. prep) and Dhungel et al. (2022).

[1] Mention of trade names or commercial products in this publication is solely for the purpose of providing specific information and does not imply recommendation or endorsement by the U.S. Department of Agriculture.

BAITSSS model

The detailed model description (BAITSSS configuration as shown in Fig. 1) and complete set of the equations utilized in the BAITSSS model can be found in Dhungel et al. (2016, 2019, 2020). This section summarizes the model and presents some primary equations. Flux gradient equations were used to compute latent heat flux (LE) and sensible heat flux (H), whereas Jarvis-type canopy resistance (r_{sc}) was used for estimating transpiration. BAITSSS estimates ET based on weather, soil moisture conditions, and canopy development (vegetation indices and physical properties), where the surface temperature required for the energy balance is computed iteratively for each time step. Irrigation (I_{rr}) in BAITSSS is triggered when root zone soil moisture (θ_{root}) falls below the threshold moisture content (θ_t),

$$I_{rr} = \begin{cases} (\theta_{fc} - \theta_{root}) d_{root} & \text{if } \theta_{root} < \theta_t \\ 0 & \text{if } \theta_{root} \geq \theta_t \end{cases} \quad (1)$$

RAW is computed based on the management allowable depletion (MAD) and total available water (TAW),

$$\text{RAW} = \text{MAD}\left(\theta_{fc} - \theta_{wp}\right) = \text{MAD} \cdot \text{TAW} \quad (2)$$

where $\text{TAW} = \theta_{fc} - \theta_{wp}$ and θ_{wp} is the wilting point soil moisture content and θ_{fc} is field capacity. In this study, a constant MAD (0.4–0.6) for entire crop growth stages was used. The threshold θ_t is computed from readily available water (RAW) and θ_{fc} (Eq. 3),

$$\theta_t = \theta_{fc} - \text{RAW} \quad (3)$$

A reduction in MAD causes a corresponding reduction in RAW and consequently increases θ_t. When MAD is equal to 1, θ_t becomes θ_{wp}, i.e., the model delays irrigating until θ_{root} becomes θ_{wp}. When $\text{MAD} = 0$ ($\theta_t = \theta_{fc}$), the model does not let the soil moisture go below θ_{fc}. Each irrigation event restores soil moisture to θ_{fc} for both the soil surface layer (d_{sur}) and the root zone layer (d_{root}) (as assumed sprinkler irrigation). Two concurrent accountings of soil moisture are made, one for the soil surface and one for the full root zone. Water content at the soil surface (θ_{sur}) (Eq. 4) is computed as

$$\theta_{sur} = \theta_{sur(i-1)} + \frac{\left(P + I_{rr} - S_{run}\right) - E_{ss} - T_e}{d_{sur}} + \text{CR}_e - \text{DP}_e \quad (4)$$

where $\theta_{sur(i-1)}$ is the volumetric water content (VWC) of the surface layer at the previous time step ($m^3\ m^{-3}$), E_{ss} is soil surface evaporation (mm), P is precipitation (mm), S_{run} is surface runoff (mm), I_{rr} is irrigation, d_{sur} (= 150 mm) is soil surface depth, DP_e is deep percolated water from the upper soil layer to the root zone ($m^3\ m^{-3}$), CR_e is capillary rise

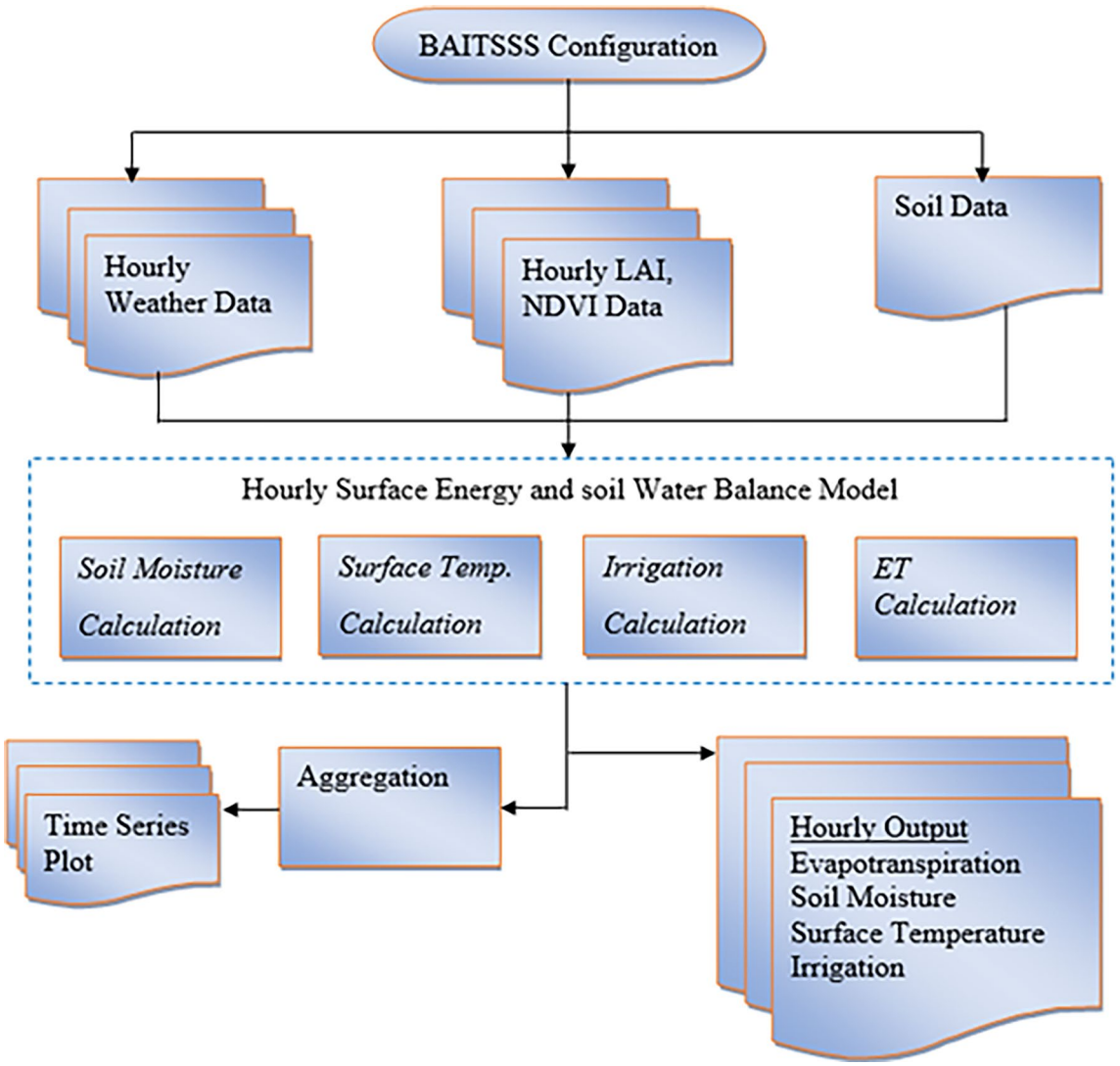

Fig. 1 BAITSSS configuration with inputs (weather, vegetation indices, and soil data), intermediate, and output

from the root zone into the first soil surface layer ($m^3\ m^{-3}$), and T_e is transpiration from the soil surface layer (mm).

The water content of the root zone (θ_{root}) is similarly evaluated as Eq. (5), where root zone control volume consists of the soil surface layer.

$$\theta_{root} = \theta_{root(i-1)} + \frac{\left(P + I_{rr} - S_{run}\right) - E_{ss} - T}{d_{root}} + CR - DP \tag{5}$$

where $\theta_{root(i-1)}$ is VWC of the root zone from previous time steps, T is transpiration from vegetation, d_{root} (=500 mm) is rooting depth for entire growth stages, DP is deep percolation below the root zone, and CR is capillary rise from the third layer to the root zone. CR_e, CR, and T_e were neglected in the present analysis to simplify the soil water balance. Currently, the model permits soil to be dry at the surface (d_{sur}) to an air-dry condition (Campbell and Norman 2000). The θ_{sur} can elevate to saturated soil moisture (θ_{sat}), while θ_{root} is limited to θ_{fc}.

A Jarvis-type equation was used to compute canopy resistance (r_{sc}) with weighting functions representing plant response to solar radiation (F_1), air temperature (F_2), vapor pressure deficit (F_3), and soil moisture (F_4) (Alfieri et al. 2008; Kumar et al. 2011),

$$r_{sc} = \frac{R_{c\_min}}{\frac{LAI}{f_c} F_1 F_2 F_3 F_4} \tag{6}$$

where LAI is leaf area index and f_c is fraction of canopy cover. The fraction of canopy cover (f_c) is calculated based on NDVI as suggested by Gutman and Ignatov (1998), Dhungel et al. (2016).

The minimum value of canopy resistance (R_{c_min}) is set at 40 sm^{-1} as per Kumar et al. (2011), Dhungel et al. (2019) for irrigated agricultural landscapes. When $F_1 = F_2 = F_3 = F_4 \sim 1$, r_{sc} becomes the minimum.

A logistic growth-type equation (W) is used to calculate the effects of the available water fraction (AWF) for F_4 in Eq. (6) (Anderson et al. 2007).

$$\mathrm{AWF} = \frac{\theta_{root} - \theta_{wp}}{\theta_{fc} - \theta_{wp}} \tag{7}$$

$$F_4 = \frac{\ln(W)}{\ln(W_f)} \tag{8}$$

$$W = \frac{W_0 W_f}{W_0 + (W_f - W_0)\exp(-\mu \mathrm{AWF})} \tag{9}$$

W_o, W_f, and μ are logistic growth equation coefficients, where $W_o = 1$, $W_f = 800$, and $\mu = 12$.

BAITSSS adjusted energy and water balance components using f_c to partition soil and canopy components.

Weather, soil, and vegetation data

The primary inputs of BAITSSS are weather, vegetation indices, and soil data (Fig. 1). Soil hydraulic characteristics data (θ_{fc} and θ_{wp}) were acquired from the area and depth-averaged NRCS soil survey database SSURGO as described by Wieczorek (2014) and were added in Table 1. AZMET (Arizona Meteorological Network) and the EC sites provided the hourly weather data. Normalized difference vegetation index (NDVI) was derived from linearly interpolated Sentinel-2 and leaf area index (LAI) was estimated from the empirical relationship relating NDVI to LAI. Relatively dry initial surface ($\theta = 0.05$ m^3 m^{-3}) and root zone ($\theta = \theta_{wp}$) soil moisture contents were considered for all sites since minimal precipitation occurred 15 days before planting (i.e., start of the simulation).

Results

Weather and vegetation indices

The average flux (diurnal cycle; 24 h) of solar radiation decreased from ~ 250 to ~ 150 W m^{-2} and air temperature decreased from ~ 30 to ~ 10 °C toward the winter solstice. During this period, vegetation indices were mostly increasing creating phase differences between solar radiation and air temperature (Fig. 2). To reduce daily scatter, Polyfit and polyval functions of the polynomial module were used within the Python-based library NumPy to smooth the

Table 1 Soil moisture characteristics and water balance components based on MAD of 0.5 of lettuce for multiple sites for various years around Yuma, AZ

S.no	Name	$Irr_{applied}$ (mm)	$Irr_{BAITSSS}$ (mm)	ET_{EC} (mm)	$ET_{BAITSSS}$ (mm)	P (mm)	θ_{fc} ($m^3 m^{-3}$)	θ_t ($m^3 m^{-3}$)	Change (I_{rr}) %	Change (ET) %
a	NGIDD 19-20a	308.6	271.9	314.1	229.1	32.3	0.19	0.10	−11	−27
b	YID 18b	274.2	304.8	247.0	251.2	17.8	0.32	0.22	11	1
c	YCWUA 18a	442.9	362.0	263.2	303.2	24.1	0.42	0.34	−18	15
d	YID 17a	257.0	300.9	269.7	238.3	0.0	0.30	0.20	17	−11
e	YID 19-20a	435.1	227.1	297.5	227.4	58.1	0.19	0.10	−47	−23
f	YCWUA 19-20a	406.8	361.3	257.4	327.5	34.3	0.42	0.34	−11	27
g	YID 17d	281.2	401.5	249.0	328.2	1.3	0.30	0.20	42	31
h	YID 17b	328.6	401.3	306.9	306.9	1.3	0.30	0.20	22	0
i	YID 17c	243.1	305.1	267.6	249.9	1.3	0.32	0.22	25	−6
j	YCWUA 17-18b	411.5	458.5	302.8	374.5	2.0	0.32	0.22	11	23
k	YCWUA 17-18a	335.3	441.6	234.1	396.8	2.0	0.42	0.34	31	69
l	YID 16	310.3	305.4	245.6	221.2	1.3	0.32	0.22	−1	−9

Data are reported for each cropping season, which varied in length

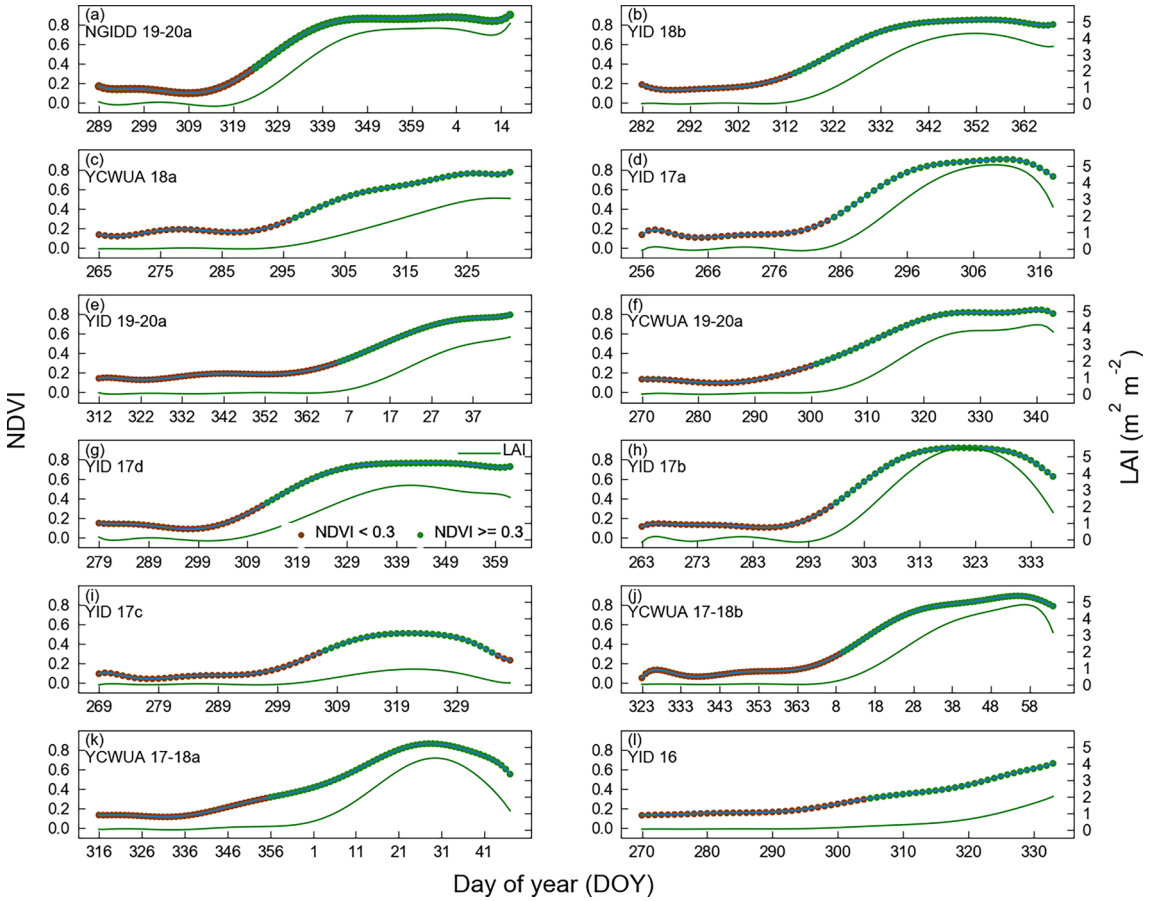

Fig. 2 Daily values of vegetation indices (LAI and NDVI) from Sentinel-2 for various sites for multiple years around Yuma, AZ

NDVI and LAI values. NDVI period (<0.3 and ≥ 0.3) were separated for differentiating bare soil and the non-vegetated period from the vegetative period (based on color code). The maximum duration when NDVI <0.3 was 58 days for the site YID 19–20a (Fig. 2e) while the minimum was 29 days for the site YID 17a (Fig. 2d) with an average value of 38 days. Lettuce harvesting is done at peak or close to peak vegetative cover. Most of the sites showed cut-off in NDVI and LAI at the peak with some exceptions. The vegetation indices showed some variability among the sites, with the maximum values of NDVI and LAI being ~ 0.9 and ~ 5.5 $m^2\ m^{-2}$, respectively. The site YID 17c had the smallest vegetation index values (Fig. 2i, maximum NDVI ~ 0.4 and LAI ~ 1 $m^2\ m^{-2}$) followed by YCWUA 17–18a (Fig. 2l, maximum NDVI ~ 0.6 and LAI ~ 2 $m^2\ m^{-2}$).

Irrigation frequency and depth

Figure 3 shows applied irrigation, precipitation, and the progression of simulated irrigation based on multiple MADs on a daily time scale. Field data showed that irrigation was generally applied on the first day of planting. Due to the assumed low initial moisture content ($=\theta_{wp}$) of the root zone, BAITSSS auto-irrigation also simulated on the first day ($\theta_{wp} < \theta_t$ at the start of simulation) for all considered MADs. The irrigation depth (mm) from BAITSSS for the first application was the largest of the simulation because the model did not let the moisture go below the θ_t thereafter (Fig. 3). For all sites, the second simulated irrigation was triggered earliest when MAD = 0.4, followed by MAD = 0.5 and MAD = 0.6. Applied irrigation in the field showed a higher frequency of small irrigation events (< 20 mm) right after planting in all sites, which were mostly on daily basis or some days apart after the first irrigation. The frequent water applications were due to sprinkler irrigation being used during crop establishment to create a cool microclimate (Sanchez et al. 2009). However, the average difference between the first and second simulated irrigation events among all sites was 13, 18, and 24 days for MAD of 0.4, 0.5, and 0.6, respectively. The shortest difference was 5 days for YCWUA 18a (Fig. 3c) for MAD of 0.4 while the longest difference was 69 days for YID 19–20a (Fig. 3e) for MAD of 0.6, which was pushed back by multiple precipitation events. It was evident that precipitation delayed both applied and

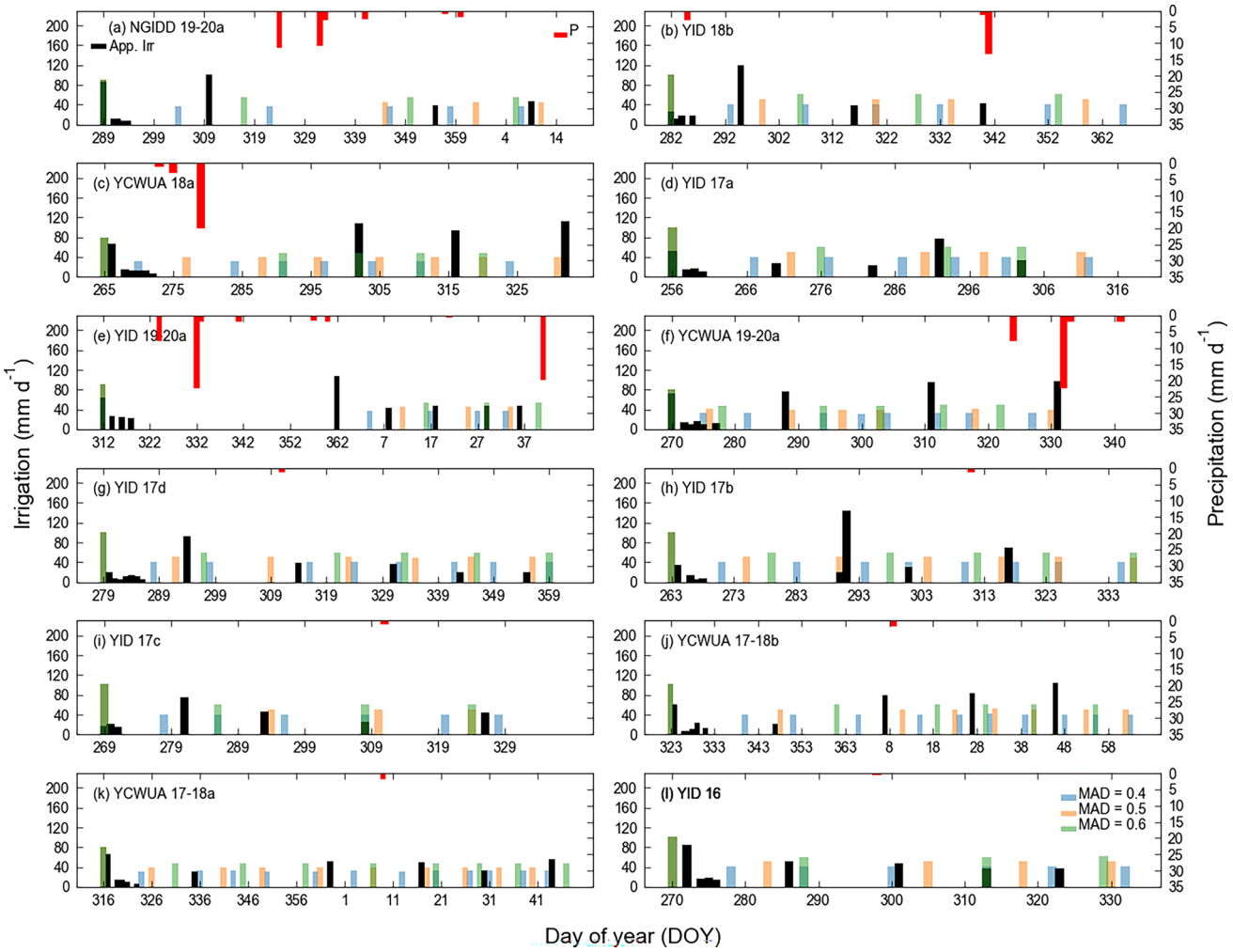

Fig. 3 Daily applied irrigation and precipitation, and progression of simulated irrigation from BAITSSS based on various management allowable depletions (MADs) around Yuma, AZ

simulated irrigation (e.g., NGIDD 19–20a, Fig. 3a, YID 19–20a, Fig. 3e). The frequency and the application depth of simulated irrigation differed from applied irrigation later in the season as well. As indicated earlier, irrigation in BAITSSS (timing and depth) was triggered based on vegetative and weather demand with predefined management scenarios. Farmers normally rely on visual inspection of the crop, historical experience based on previous seasons, their knowledge about soil water retention, and energy cost. The applied irrigation depth varied from < 20 to > 80 mm.

Evapotranspiration time series

Visual inspection of daily ET data (Fig. 4) showed that BAITSSS simulated ET closely followed EC measured values. However, differences were evident during the partial cover period mainly due to soil evaporation (YID 17a, Fig. 4d; YCWUA 19–20a, Fig. 4f; YID 17b, Fig. 4h). The ET spikes from BAITSSS followed the simulated irrigation based on the respective MADs. The mismatch between EC and BAITSSS daily ET spikes was generally smaller during the full cover period, though it was not completely eliminated (YID 17d, Fig. 4g; YCWUA 17–18a, Fig. 4k). Obviously, the simulated ET when using applied irrigation [ET (App.Irr)] data as inputs was in closer agreement with EC measurements compared to simulated irrigation (Fig. 4). Eddy covariance measured evapotranspiration [ET (EC)] generally stayed higher right after planting because of the multiple small irrigation events, whereas ET predicted from BAITSSS showed a decline after the first irrigation event due to larger gaps in simulated irrigation events (NGIDD 19–20a, Fig. 4a; YID 17a, Fig. 4d). The maximum daily ET value was ~ 8 mm from both EC and BAITSSS (YID 17b, Fig. 4h); however, ET was generally less than 6 mm most of the time. Evapotranspiration from EC for YCWUA 17–18a (Fig. 4k) was unrealistically stable (~ 3 mm) and

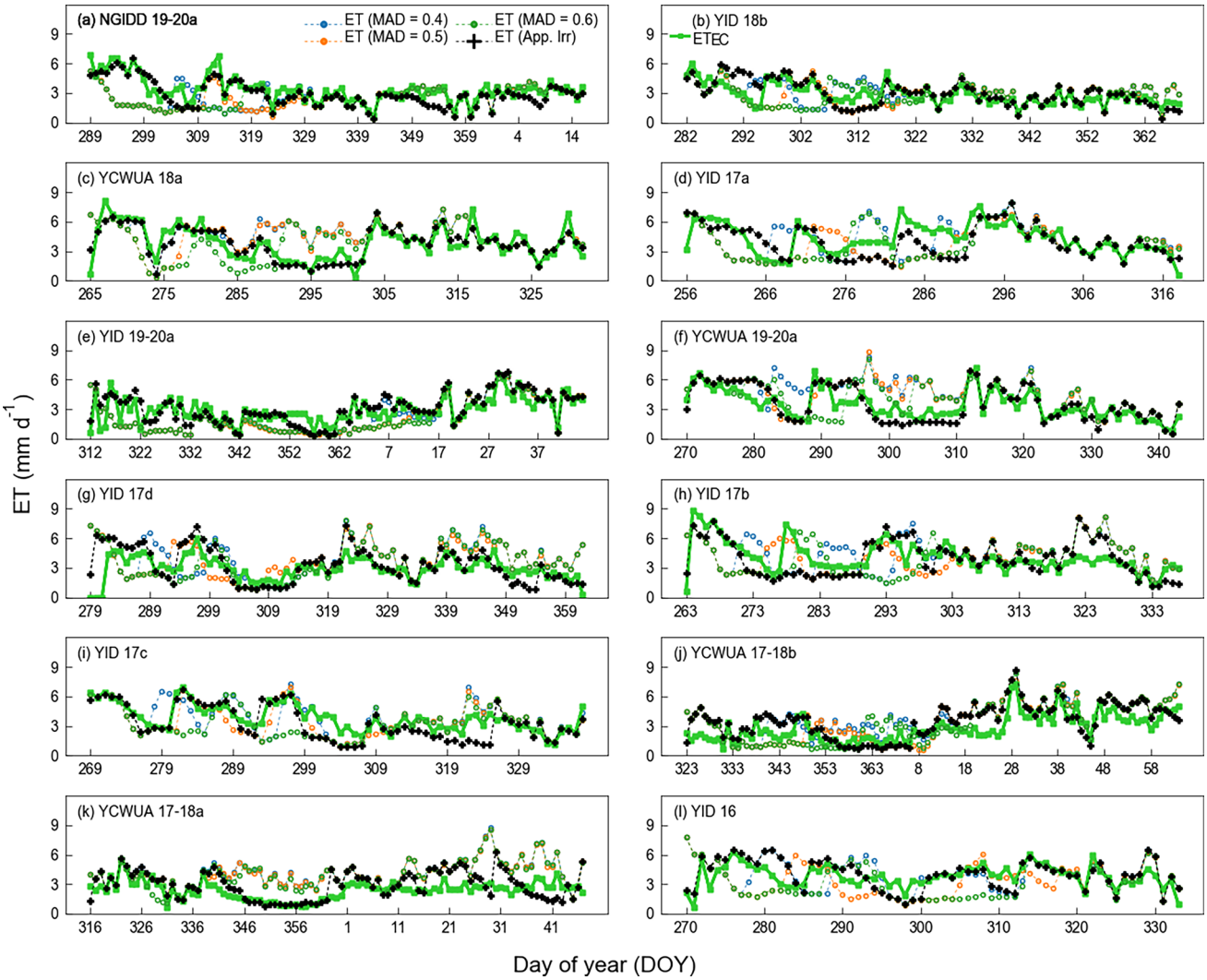

Fig. 4 Daily evapotranspiration (ET) for irrigated lettuce at various sites around Yuma, AZ. ET_{EC} is ET measured with eddy covariance, $ET_{BAITSSS}$ is ET simulated with BAITSSS using irrigation data as input, and the remaining curves are ET simulated with BAITSSS using various levels of management allowable depletion (MAD) to trigger simulated irrigation

less responsive to irrigation events after the new year than BAITSSS ET.

Soil moisture at root and F_4

Figure 5 shows the relationship between F_4 and θ_{root} based on the logistic equation (Eqs. 7–9). The gradual change in shape and the transition points of these curves provide the basis for triggering irrigation. The upper value of soil moisture on the horizontal axis of each plot is field capacity, whereas the lower value was threshold moisture content (Fig. 5). NGIDD 19–20a (Fig. 5a) and YID 19–20a (Fig. 5e) had the lowest field capacity (θ_{fc}) of 0.19 m^3 m^{-3}, while YCWUA 18a (Fig. 5c), YCWUA 19–20a (Fig. 5f), and YCWUA 17–18a (Fig. 5k) had the highest θ_{fc} of 0.42 m^3 m^{-3}. As per the irrigation rules, the model does not permit the soil moisture to go below θ_t to avoid moisture-related stress and each irrigation event brings moisture back to θ_{fc} (Fig. 3). The F_4-θ_{root} curves for individual MADs overlap each other for individual sites because of the identical shape of AWF (θ_{wp}, θ_{fc}). The F_4 reached the upper limit i.e., ~ 1 when $\theta_{root} = \theta_{fc}$ for all MADs. The lowest value of F_4 was ~ 0.9, ~ 0.85 ~ 0.7 for MADs of 0.4, 0.5, and 0.6, respectively. As a reminder, higher values of the weighing functions F_1, F_2, F_3, and F_4 create lower r_{sc} and ultimately smaller resistance to transpiration.

The simulated root zone soil moisture (θ_{root}) is shown in Fig. 6. The soil moisture time course corresponded to the progression of MAD-based irrigation shown in Fig. 3 and ET spikes shown in Fig. 4. The first irrigation event at the start of the simulation restored θ_{root} to θ_{fc} in all sites. The subsequent, i.e., second irrigation (excluding the start

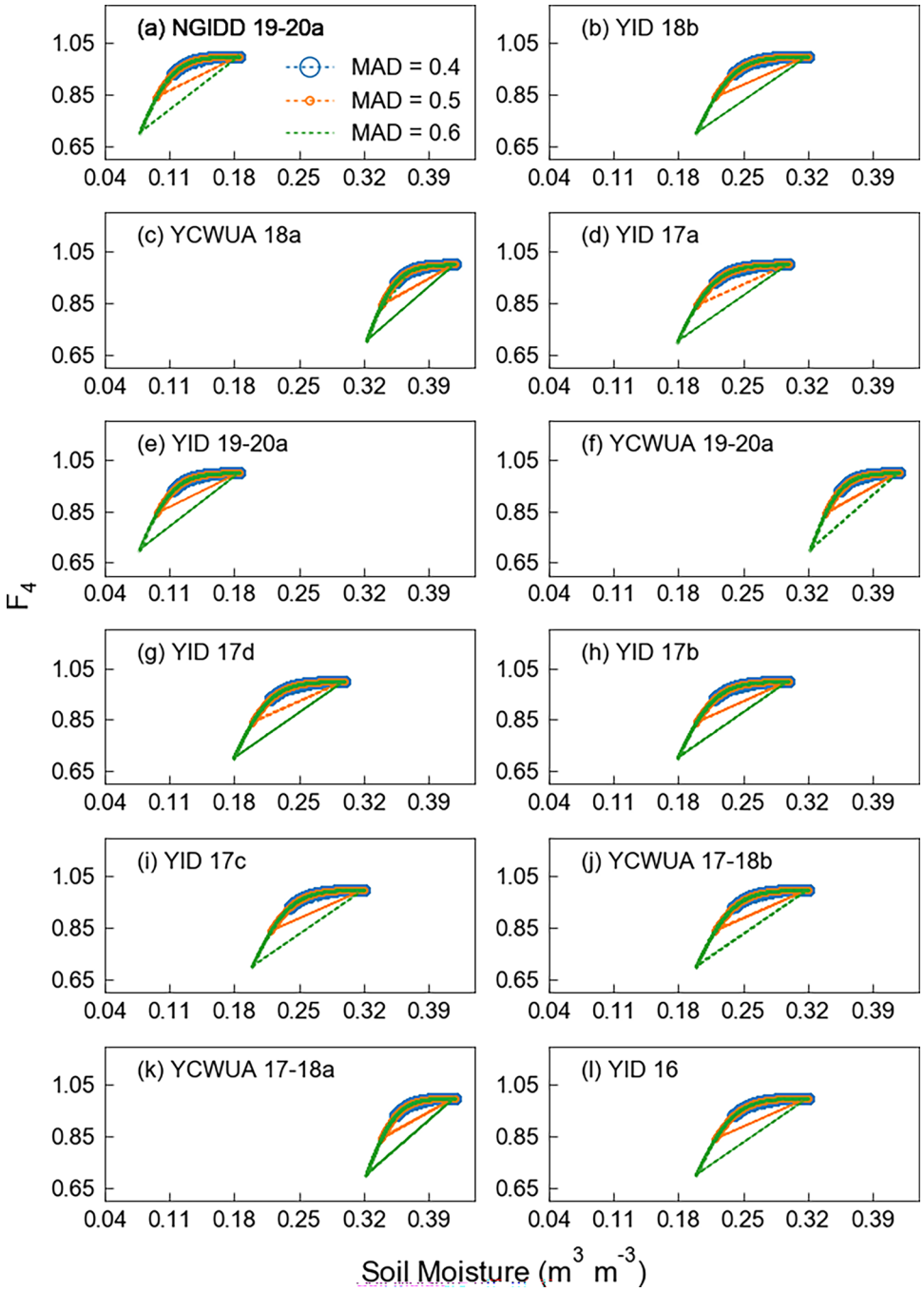

Fig. 5 Hourly weighting functions relating plant response (F_4) to root zone soil moisture θ_{root} for various sites around Yuma, AZ. The straight line connecting the endpoints was added to help distinguish three curves in each plot

of simulation) was trigged first for MAD = 0.4 and last for MAD = 0.6. The θ_{sur} followed a similar trend of θ_{root} i.e., continuously decreased until the next irrigation or precipitation occurred (not shown).

Seasonal cumulative evapotranspiration

A comparison of seasonal ET between EC and BAITSSS showed mixed results (Fig. 7). For instance, some sites showed good agreement (within ± 10%) (YID 18b, Fig. 7b; YID 17a, Fig. 7d; YID 17b, Fig. 7h; YID 17c, Fig. 7i; YID 16, Fig. 7l); some had positive bias (YCWUA 18a, Fig. 7c; YCWUA 19–20a, Fig. 7f; YID 17d, Fig. 7g; YCWUA 17–18b, Fig. 7j; YCWUA 17–18a, Fig. 7k), while others had negative bias as well (NGIDDD 19–20a, Fig. 7a; YID 19–20a, Fig. 7e). The % values in the legend of each plot indicate the difference between simulated and measured cumulative ET from EC when BAITSSS was run with a MAD of 0.5 (Table 1). The largest positive bias was 69% for YCWUA 17–18a (Fig. 7k) while the largest negative

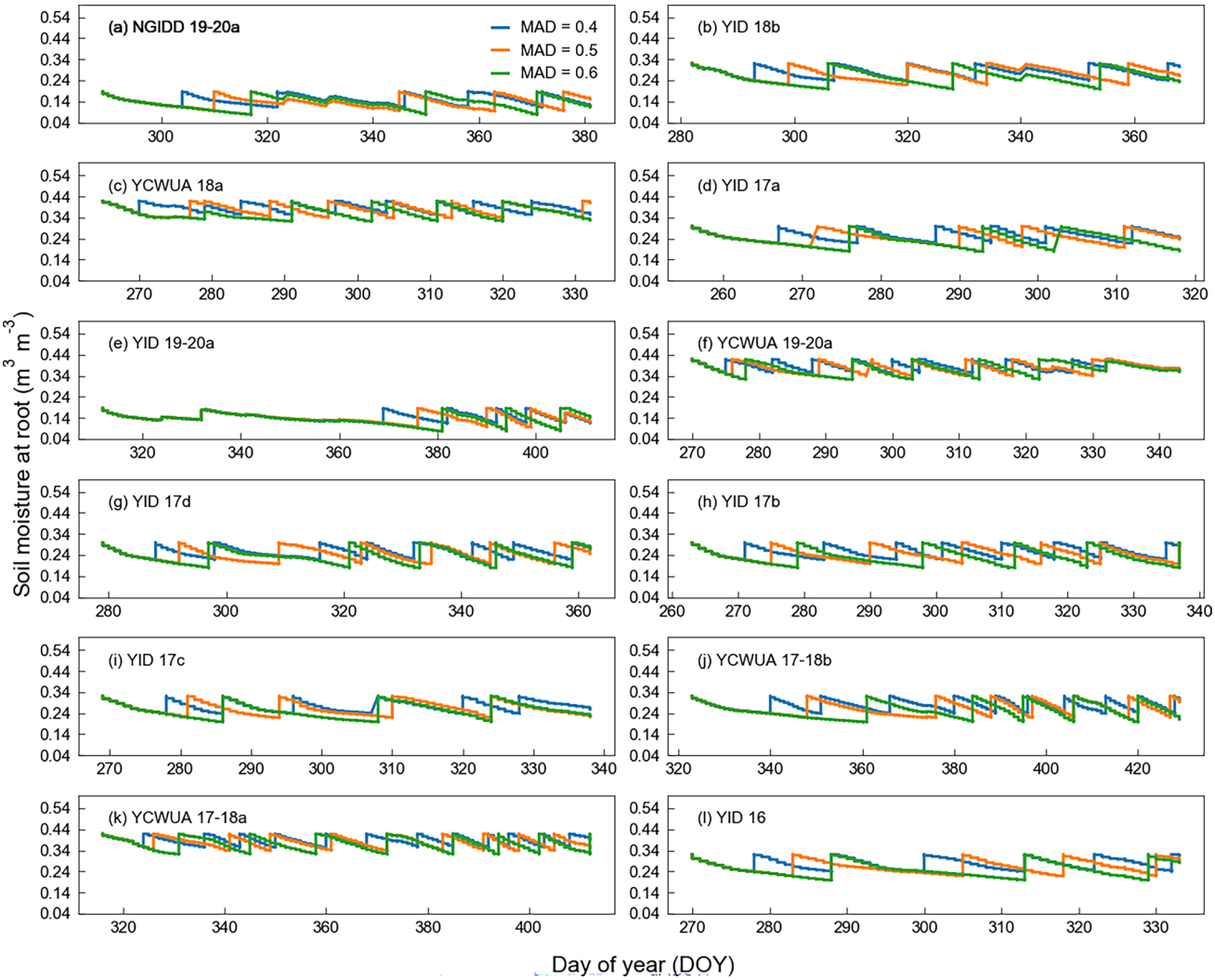

Fig. 6 Estimated daily root zone soil moisture from BAITSSS for various sites around Yuma, AZ

bias was −27% for NGIDD 19–20a (Fig. 7a). For YCWUA 17–18a, unrealistically stable ET from EC, (i.e., less responsive to irrigation events during the latter part of the simulation after the start of the new year) led to the large differences. For BAITSSS simulations with MAD = 0.5, the average difference between BAITSSS and EC cumulative ET was 7% over all sites and years. The average difference dropped to 2% when NGIDD 19–20a was excluded from the analysis. The MAD producing the best cumulative ET agreement varied by site. As expected, seasonal ET from BAITSSS was largest from MAD = 0.4 and smallest from MAD = 0.6 in all sites due to fewer irrigation events and less soil evaporation as MAD increases. The largest difference between the seasonal ET values between MAD of 0.4 and 0.6 was 19% for YID 16 (Fig. 7l), while the lowest difference was 2% for NGIDD 19–20a with average of ~ 10% among the sites.

We further assessed cumulative ET by separating the period when the soil evaporation was dominant (NDVI < 0.3) and afterward (Fig. 8). It was interesting to see that some sites showed better agreement during the period NDVI < 0.3 (YID 18b, YCWUA 18a, YID 17d, YCWUA 17–18b) while other showed during NDVI > 0.3 (NGIDD 19–20a, YID 17a, YID 19–20a, YID 17c, YID 16). The largest negative bias between EC and BAITSSS seasonal ET (−49%) occurred when NDVI < 0.3 at the sites with the largest underestimation of seasonal ET (Figs. 7a, e and 8a, e, respectively). These sites had nominal differences in cumulative ET (−6% to −1%, respectively) during the period when NDVI > 0.3. Conversely, the largest positive bias during the period when NDVI < 0.3 was 54%, and 79% during the period when NDVI > 0.3 for YCWUA 17–18a. This site was the largest contributor to the seasonal ET difference between EC and BAITSSS (Fig. 7k).

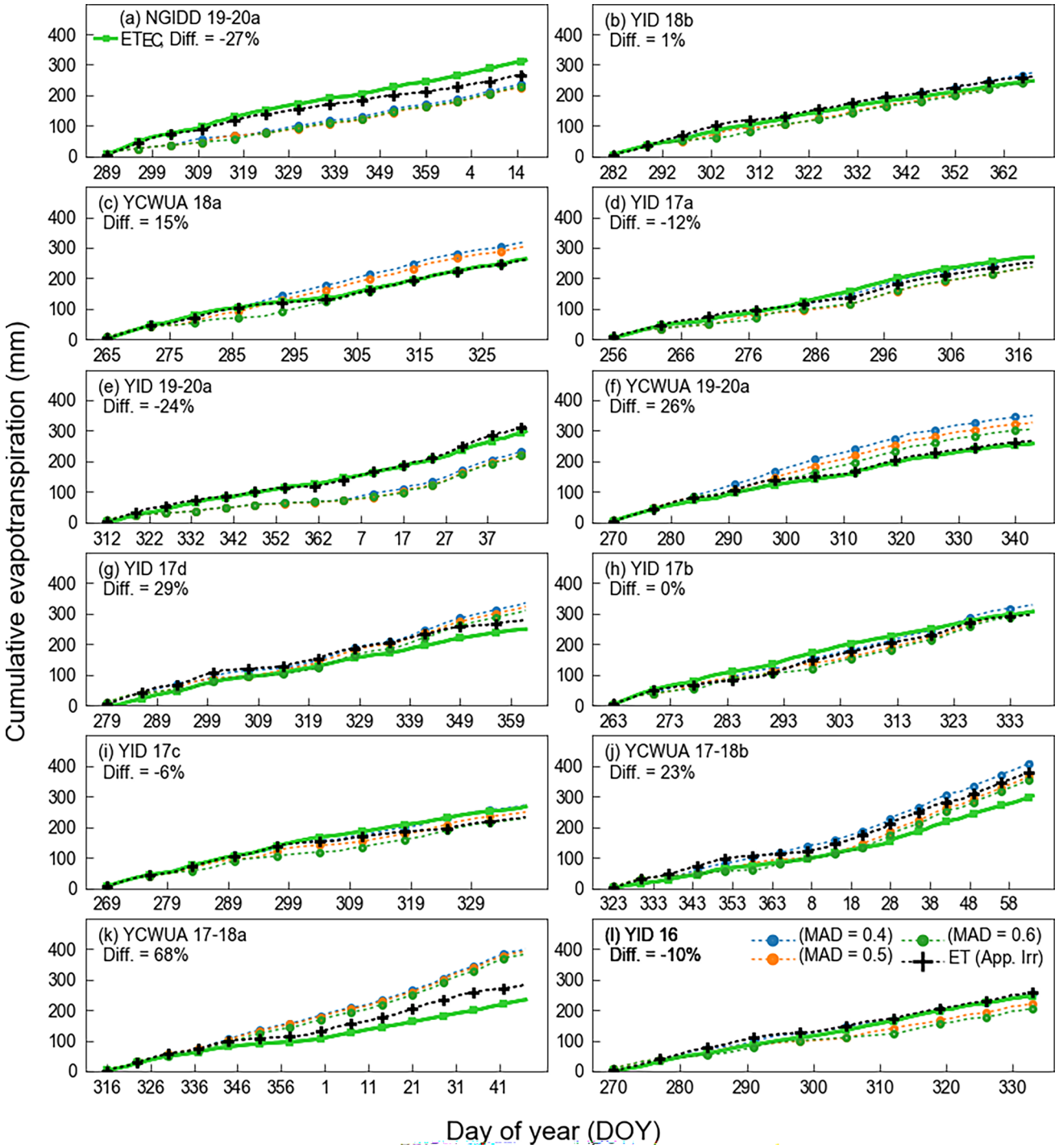

Fig. 7 Cumulative seasonal ET from EC and BAITSSS of lettuce for various sites Yuma, AZ. Percent difference (Diff.) is based on MAD of 0.5

Seasonal cumulative irrigation

Applied and simulated cumulative seasonal irrigation agreed well at some sites (NGIDD 19–20a, Fig. 9a; YID 18b, Fig. 9b; YCWUA 19–20a, Fig. 9f; YCWUA 17–18b, Fig. 9j; YID 16, Fig. 9l) and less well at others (Table 1). As an interesting fact, differences between simulated and measured seasonal ET at sites NGIDDD 19–20a (Fig. 7a) and YID 19–20a (Fig. 7e) were of similar magnitude (both around − 25%) with MAD = 0.5 (Fig. 9). In contrast, the corresponding differences in seasonal irrigation differed significantly around − 11% for NGIDDD 19–20a (Fig. 9a) and around −47% for YID 19–20a (Fig. 9e) although both showed negative bias. Seasonal

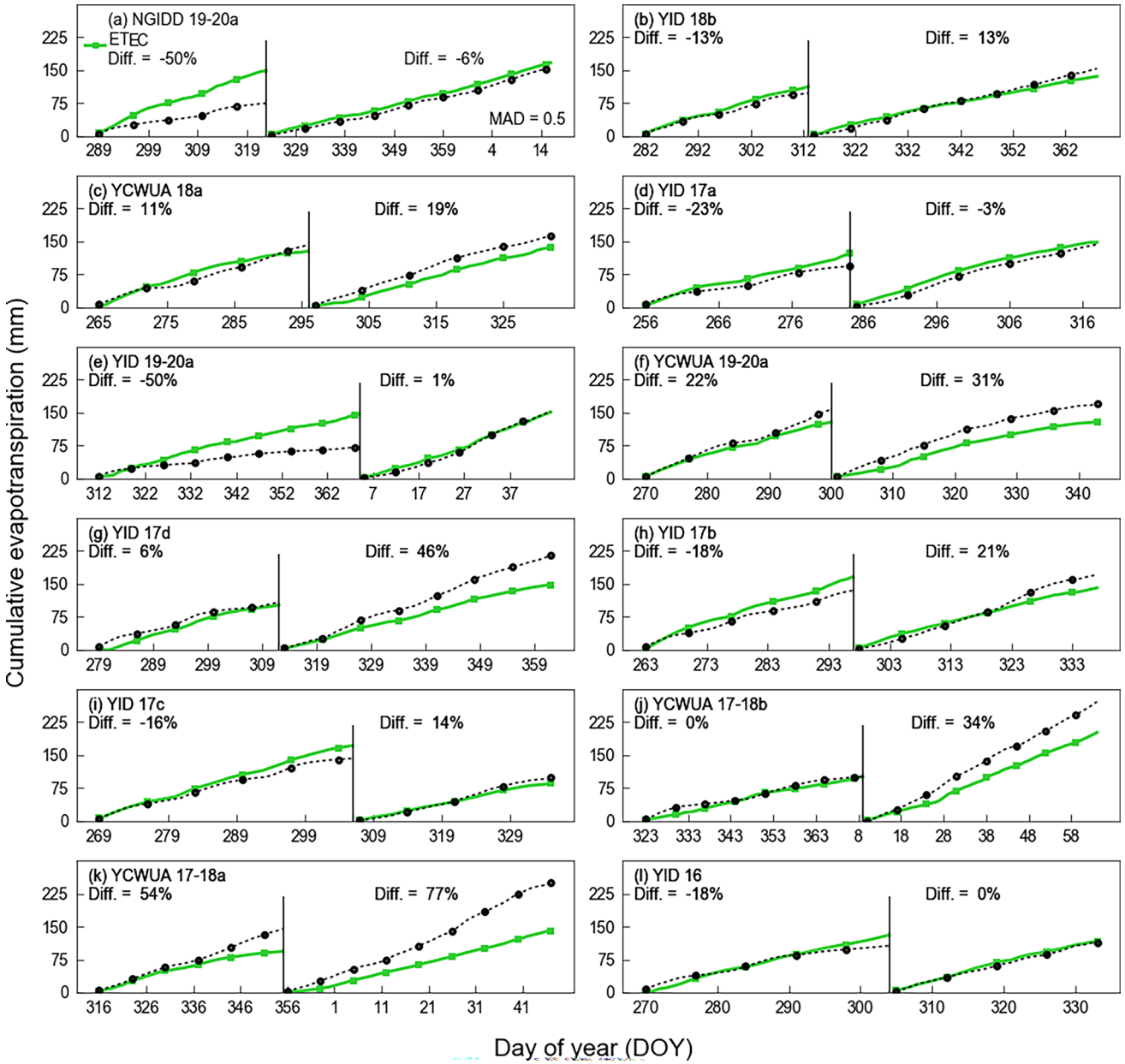

Fig. 8 Cumulative seasonal ET from EC and BAITSSS for lettuce at various sites around Yuma, AZ. The two periods in each plot are the period when soil evaporation was dominant (NDVI < 0.3) and afterward. Percent difference (Diff.) is based on MAD of 0.5

precipitation was similar at both sites (32 mm for NGIDD 19–20a and 58 mm for YID 19–20a). The variability of seasonal irrigation among the MADs was also small for both of these sites (NGIDDD 19–20a and YID 19–20a) and both had identical soil moisture characteristics with the lowest θ_{fc} among all sites, 0.19 m^3 m^{-3}. Applied irrigation similar to or smaller than simulated (i.e., a positive bias) generally indicates efficient water application (YID 18b, YID 17a, YID 17d, YID 17b, YID 17c, YCWUA 17–18b). The maximum positive bias (42%) in cumulative irrigation was for YID 17d (Fig. 7g; Table 1). The mean seasonal differences between simulated and applied irrigation among the sites and years were 6%, which was close to seasonal cumulative ET (7%). Like cumulative ET, simulated cumulative irrigation was largest for MAD of 0.4. The largest difference between the seasonal irrigation values among the sites between MAD of 0.4 and 0.6 was 20% for YCWUA 17–18b (Fig. 9j), while the lowest difference was −7% for YID 19–20a (Fig. 9e) with average of ~ 10%.

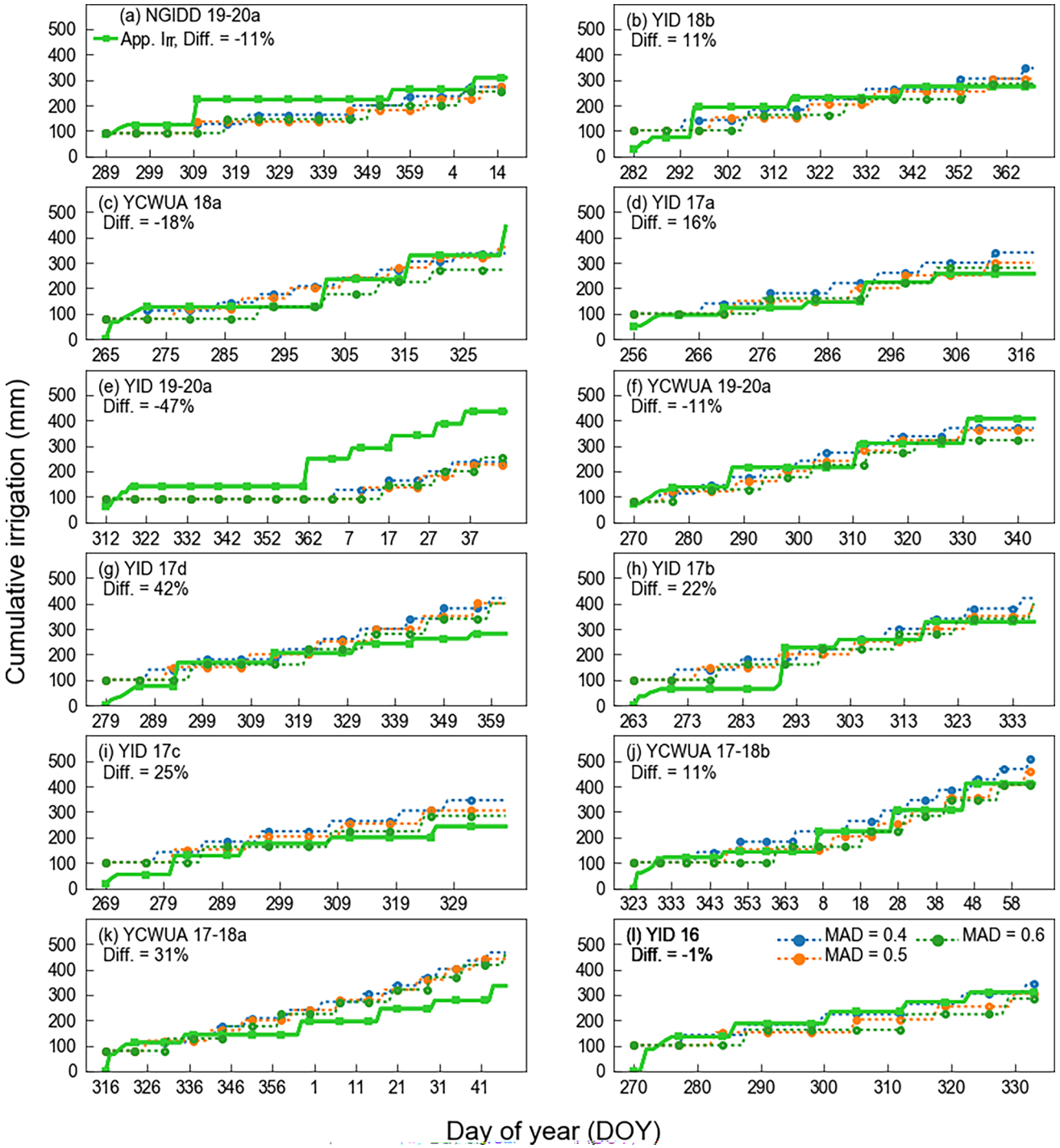

Fig. 9 Cumulative seasonal irrigation of lettuce for various sites around Yuma, AZ. Percent difference (Diff.) is based on MAD of 0.5

Accuracy assessment

Figure 10 presents scatterplots between EC and BAITSSS simulated daily ET where points lie on both sides of the 1:1 line. However, larger differences were observed during the partial cover period in some sites (NDVI < 0.3 indicated by a smaller brown color circle symbol and afterward a larger green symbol). As observed in Fig. 4, the BAITSSS ET showed a continuous decline after the first irrigation event, i.e., right after planting and during the crop establishment period, whereas EC ET mostly stayed high due to frequent, small irrigation events. These different irrigation patterns were a primary cause of differences in ET during that period. The higher agreement (points close to 1:1) during

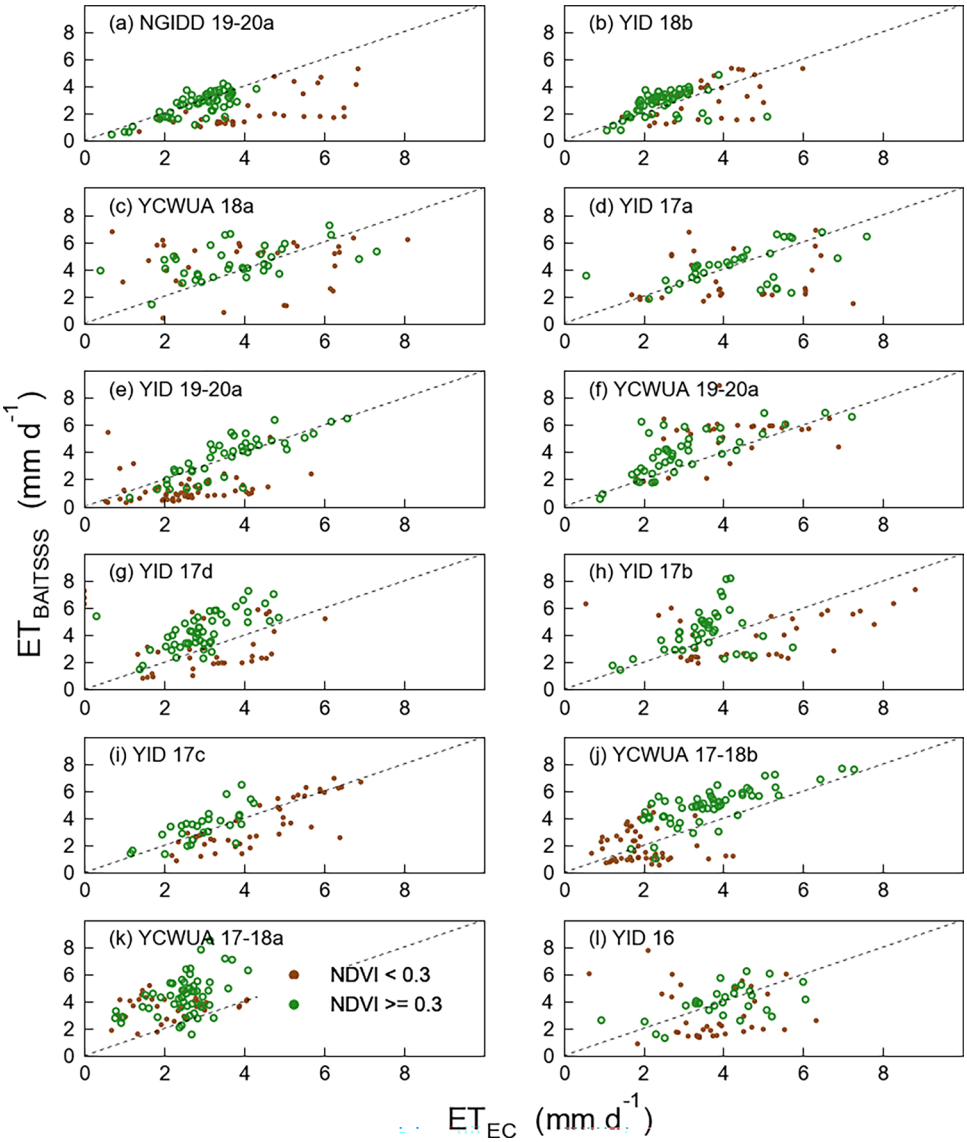

Fig. 10 Scatterplot of daily evapotranspiration (ET) derived from eddy covariance (ET_{EC}) versus ET computed with BAITSSS ($ET_{BAITSSS}$). The BAITSSS model was run using a management allowable depletion (MAD) of 0.5. The results are for various lettuce fields around Yuma, AZ

the latter part (mostly during the full cover period) was perhaps because evaporation was less influential, and also because ET may have attained near reference conditions. BAITSSS didn't compute reference ET (ET_o) based on the FAO-56 method (Allen et al. 1998), instead, the minimum canopy resistance (r_{sc}) of 40 sm^{-1} limits the maximum value of transpiration.

Discussion

A major advantage of remote sensing-based energy balance ET models is that there is no direct need for ground-based moisture conditions and does not require irrigation. Limited studies have been done utilizing remote sensing-based energy balance to simulate irrigation and compare it to applied irrigation applications. For instance, Droogers et al. (2010) estimated applied irrigation application with reasonable accuracy (95%) by remotely sensed evapotranspiration observations (Landsat) provided that data are available at an interval of 15 days or shorter and the accuracy of the signal is 90% or higher. METRIC (Allen et al. 2007), a widely used remote sensing-based energy balance model, incorporates precipitation-based soil water balance to evaluate the upper soil moisture condition of hot pixel (Allen et al. 2013; Tasumi 2019). However, neither applied nor simulated irrigation is accounted for in these water balance as this information is not readily available. Chen et al. (2018) and Taghvaeian et al. (2020) documented hydrological and crop growth models that had the capability of irrigation simulation (manual and auto-irrigation) which were Soil and Water Assessment Tool (SWAT; watershed scale model) (Arnold et al. 1998), the Agricultural Policy/Environmental eXtender (APEX; small watershed/field-scale

model) (Williams 1995), the Decision Support System for Agrotechnology Transfer (DSSAT; crop model) (Jones et al. 2003), Root Zone Water Quality Model (RZWQM; field-scale model) (Ahuja et al. 2000), MODFLOW (groundwater model) (McDonald and Harbaugh 1988), and AquaCrop (Raes et al. 2009).

SWAT and APEX models had auto-irrigation which is either based on a water stress identifier of either plant water demand or soil water content. Chen et al. (2018) further developed auto-irrigation algorithms for the SWAT model based on uniform, single-season MAD as well as growth stage-specific MAD with options for seasonal growth stage partitioning based on the scheduled date and accumulated heat units. They indicated improved model performance for simulations of irrigation amount and frequency and actual evapotranspiration compared with observed data from an irrigated lysimeter field. Some other studies also indicated promising results for detection irrigation applications using microwave in some regions, however, because of spatial mismatch between model and satellite data, effects of topography, vegetation, frozen soils, and Radio-frequency Interference (RFI) led to substantial uncertainties in others (Kumar et al. 2015; Massari et al. 2021).

The irrigation depth in BAITSSS depends on the rooting depth, MAD, and soil moisture characteristics, along with vegetation cover and weather demand. A constant rooting depth of 500 mm (relatively shorter than for grain crops) and a constant MAD were adopted for the entire simulation period. Excluding the first irrigation event (at the start of the simulation), the rest of the irrigation depths from BAITSSS was nearly identical (because of identical θ_t) for a given MAD. During crop establishment and early growing periods, rooting depths are shallower than those at maturity, i.e., full canopy cover. In addition, applied irrigation showed that MAD right after planting can be significantly smaller compared to the later period. Implementing dynamic rooting depth (a gradual increase of rooting depth mimicking root growth) as implemented by Song et al. (2013), El Masri et al. (2015), Liu et al. (2020) in land surface models and growth stage-specific MAD may help to increase the frequency of irrigation right after planting, though it may increase computational challenges when using high spatial and temporal resolution data at the landscape scale.

Additionally, the planting dates and rooting depth may also vary based on crop types which may not be available. Because of these limitations, it is preferred to have a generalized solution from BAITSSS that can accommodate multiple crop types with fewer field data requirements. In future, with the help of high-resolution remote sensing products like Planet (Planet 2017) (daily scale, 3–5 m), soil maps like Polaris (30 m) (Chaney et al. 2016), shortwave-infrared-based water index (Yue et al. 2019), ingesting thermal band and microwave as well as combining multiple bands (for instance near-infrared and blue bands) may assist in improving/identifying these field-scale moisture conditions and irrigation. In this study, we didn't intend to revise simulated irrigation to match the applied irrigation as one of the objectives of this study was to understand the irrigation practices and behavior of farmers and growers as well as MAD-based irrigation.

Earlier study discussed that one of the primary controls on ET was solar radiation and air temperature where ET decreased toward the winter solstice and increased afterward into the new calendar year (Dhungel et al. 2022). During that period, vegetation indices were generally increasing creating phase differences with solar and air temperature. We also found similar behavior in this study (Fig. 4). We did not observe a significant underestimation of ET based on these implemented MADs from moisture-related stress. A higher value of MAD delays the irrigation, thus pushing θ_t near to θ_{wp} ($\theta_t = \theta_{wp}$ when MAD = 1). Even though ET estimated from BAITSSS appeared to be similar among the MADs during the full cover, delaying irrigation during germination and crop establishment cover period would not be realistic for healthy crop growth. Evaluating applied irrigation during the crop establishment period where a cooler micro-climate was created by frequent irrigation for the crop's physiological demand, the irrigation from BAITSSS may need to be adjusted if intended to match field conditions.

Conclusion

We evaluated ET and auto-irrigation from BAITSSS for multiple sites and years for lettuce in an arid environment. The results showed the model was competent for estimating ET utilizing MAD based on auto-irrigation. A constant rooting depth of 500 mm and constant MAD (0.4–0.6) for all crop growth stages were evaluated. The model-simulated auto-irrigation and ET based on predefined irrigation rules (MADs), soil moisture characteristics, weather, and vegetation indices. It produced mixed results where obvious differences in ET spikes were observed in some sites during the partial cover period due to variations in irrigation patterns and frequencies. The differences in ET were generally reduced during the full cover period, which may be due to the reduced effect of soil evaporation. The agreement between applied and simulated irrigation showed the model's capability as well as effective irrigation application in the field. However, fields with significantly larger applied irrigation compared to simulated may guide farmers/producers for effective irrigation application. The behavior of applied irrigation, i.e., timing and depth widely varied for the same season (< 20 to > 80 mm) when compared simulated MAD-based irrigation. One of the common behaviors of applied irrigation in all sites was a larger irrigation

frequency of small irrigation events (< 20 mm) during the initial growing period for creating a cooler microclimate. However, due to constant rooting depth, constant MAD for entire growth stages, and a longer partial cover period (average of 38 days when NDVI < 0.3) the model was unable to mimic this behavior in some sites. Overall, there was not an obvious MAD value to be chosen to model the fields absent grower provided irrigation times and depths. However, shallower rooting depth or smaller MAD value, or a combination of both can help to increase the frequency of irrigation right after planting. The average difference between both seasonal ET and irrigation was ~ 10% between MAD of 0.4 and 0.6. The study highlighted the capabilities and limitations of model-simulated auto-irrigation and ET.

Acknowledgements This work is supported by Agriculture and Food Research Initiative Competitive Grant no. 2020-69012-31914 from the USDA National Institute of Food and Agriculture. This research was supported in part by the U.S. Department of Agriculture, Agricultural Research Service (project numbers 2036-61000-018-000-D and 2020-13660-008-000-D). This research used resources provided by the SCINet project of the USDA Agricultural Research Service, ARS project number 0500-00093-001-00-D. The U.S. Department of Agriculture prohibits discrimination in all its programs and activities on the basis of race, color, national origin, age, disability, and where applicable, sex, marital status, familial status, parental status, religion, sexual orientation, genetic information, political beliefs, reprisal, or because all or part of an individual's income is derived from any public assistance program (Not all prohibited bases apply to all programs). Persons with disabilities who require alternative means for communication of program information (Braille, large print, audiotape, etc.) should contact USDA's TARGET Center at (202) 720-2600 (voice and TDD). To file a complaint of discrimination, write to USDA, Director, Office of Civil Rights, 1400 Independence Avenue, S.W., Washington, D.C. 20250-9410, or call (800) 795-3272 (voice) or (202) 720-6382 (TDD). USDA is an equal opportunity provider and employer.

Author contributions RD, RGA, AF, and TS designed and performed research, analyzed data, and originated manuscript; TS, MS and CAS contributed data; ES guided project development. All authors reviewed and revised the manuscript.

Data availability Weather data can be found (https://ag.arizona.edu/azmet/). We thank the United States Department of Agriculture (USDA) Agricultural Research Service (ARS) and the University of Arizona for providing the Eddy Covariance data.

Declarations

Conflict of interest The authors declare no conflicts of interest relevant to this study.

References

Ahuja L, Rojas KW, Hanson JD (2000) Root zone water quality model: modelling management effects on water quality and crop production. Water Resources Publication, USA

Akbar R, Short Gianotti D, McColl KA et al (2018) Hydrological storage length scales represented by remote sensing estimates of soil moisture and precipitation. Water Resour Res 54:1476–1492. https://doi.org/10.1002/2017WR021508

Alfieri JG, Niyogi D, Blanken PD et al (2008) Estimation of the minimum canopy resistance for croplands and grasslands using data from the 2002 international H_2O project. Mon Weather Rev 136:4452–4469. https://doi.org/10.1175/2008MWR2524.1

Allen RG, Pereira LS, Raes D, Smith M (1998) Crop evapotranspiration—guidelines for computing crop water requirements–FAO irrigation and drainage paper 56. FAO, Rome 300:D05109

Allen RG, Tasumi M, Morse A, Trezza R (2005) A Landsat-based energy balance and evapotranspiration model in Western US water rights regulation and planning. Irrig Drain Syst 19:251–268

Allen RG, Tasumi M, Trezza R (2007) Satellite-based energy balance for mapping evapotranspiration with internalized calibration (METRIC)—model. J Irrig Drain Eng 133:380–394

Allen RG, Burnett B, Kramber W et al (2013) Automated calibration of the METRIC-Landsat evapotranspiration process. JAWRA J Am Water Resour Assoc 49:563–576. https://doi.org/10.1111/jawr.12056

Anderson RG, Wang D (2014) Energy budget closure observed in paired Eddy covariance towers with increased and continuous daily turbulence. Agric for Meteorol 184:204–209. https://doi.org/10.1016/j.agrformet.2013.09.012

Anderson MC, Norman JM, Mecikalski JR et al (2007) A climatological study of evapotranspiration and moisture stress across the continental United States based on thermal remote sensing: 1. Model formulation. J Geophys Res Atmos. https://doi.org/10.1029/2006JD007506

Anderson MC, Allen RG, Morse A, Kustas WP (2012) Use of Landsat thermal imagery in monitoring evapotranspiration and managing water resources. Remote Sens Environ 122:50–65. https://doi.org/10.1016/j.rse.2011.08.025

Arguez A, Durre I, Applequist S et al (2012) NOAA's 1981–2010 U.S. climate normals: an overview. Bull Am Meteorol Soc 93:1687–1697. https://doi.org/10.1175/BAMS-D-11-00197.1

Arnold JG, Srinivasan R, Muttiah RS, Williams JR (1998) Large area hydrologic modeling and assessment part I: model development 1. JAWRA J Am Water Resour Assoc 34:73–89

Bartlett AC, Andales AA, Arabi M, Bauder TA (2015) A smartphone app to extend use of a cloud-based irrigation scheduling tool. Comput Electron Agric 111:127–130. https://doi.org/10.1016/j.compag.2014.12.021

Brocca L, Ciabatta L, Massari C et al (2017) Soil moisture for hydrological applications: open questions and new opportunities. Water 9:140. https://doi.org/10.3390/w9020140

Callison D (2012) Management allowed depletion irrigation scheduling, p 40. http://awqa.org/wp-content/toolkits/IrrigationScheduling/ManagementAllowedDepletion-IrrigationScheduling.pdf. Accessed 23 Jan 2023

Campbell GS, Norman JM (2000) An introduction to environmental biophysics. Springer Science & Business Media, New York

Chaney NW, Wood EF, McBratney AB et al (2016) POLARIS: a 30-meter probabilistic soil series map of the contiguous United States. Geoderma 274:54–67. https://doi.org/10.1016/j.geoderma.2016.03.025

Chen Y, Marek GW, Marek TH et al (2018) Improving SWAT auto-irrigation functions for simulating agricultural irrigation management using long-term lysimeter field data. Environ Model Softw 99:25–38. https://doi.org/10.1016/j.envsoft.2017.09.013

Clark GA (2000) KanSched an ET-based irrigation scheduling tool for Kansas summer annual crops, p 10. https://www.ksre.k-state.edu/irrigate/reports/Rogers2.pdf. Accessed 23 Jan 2023

Collow TW, Robock A, Basara JB, Illston BG (2012) Evaluation of SMOS retrievals of soil moisture over the central United States with currently available in situ observations: evaluation of SMOS

with in situ data. J Geophys Res. https://doi.org/10.1029/2011JD017095
de Vito R, Portoghese I, Pagano A et al (2017) An index-based approach for the sustainability assessment of irrigation practice based on the water-energy-food nexus framework. Adv Water Resour 110:423–436. https://doi.org/10.1016/j.advwatres.2017.10.027
Dhungel R, Allen RG, Trezza R, Robison CW (2016) Evapotranspiration between satellite overpasses: methodology and case study in agricultural dominant semi-arid areas: time integration of evapotranspiration. Met Apps 23:714–730. https://doi.org/10.1002/met.1596
Dhungel R, Aiken R, Colaizzi PD et al (2019) Evaluation of uncalibrated energy balance model (BAITSSS) for estimating evapotranspiration in a semiarid, advective climate. Hydrol Process 33:2110–2130. https://doi.org/10.1002/hyp.13458
Dhungel R, Aiken R, Lin X et al (2020) Restricted water allocations: landscape-scale energy balance simulations and adjustments in agricultural water applications. Agric Water Manage 227:105854. https://doi.org/10.1016/j.agwat.2019.105854
Dhungel R, Aiken R, Evett SR et al (2021) Energy imbalance and evapotranspiration hysteresis under an advective environment: evidence from lysimeter, eddy covariance, and energy balance modeling. Geophys Res Lett. https://doi.org/10.1029/2020GL091203
Dhungel R, Anderson R, French AN et al (2022) Assessing evapotranspiration in a Lettuce crop with a two-source energy balance model. Irrig Sci. https://doi.org/10.1007/s00271-022-00814-x
Droogers P, Immerzeel WW, Lorite IJ (2010) Estimating actual irrigation application by remotely sensed evapotranspiration observations. Agric Water Manage 97:1351–1359. https://doi.org/10.1016/j.agwat.2010.03.017
El Masri B, Shu S, Jain AK (2015) Implementation of a dynamic rooting depth and phenology into a land surface model: evaluation of carbon, water, and energy fluxes in the high latitude ecosystems. Agric for Meteorol 211–212:85–99. https://doi.org/10.1016/j.agrformet.2015.06.002
Escarabajal-Henarejos D, Molina-Martínez JM, Fernández-Pacheco DG, García-Mateos G (2015) Methodology for obtaining prediction models of the root depth of lettuce for its application in irrigation automation. Agric Water Manage 151:167–173. https://doi.org/10.1016/j.agwat.2014.10.012
Falge E, Baldocchi D, Olson R et al (2001) Gap filling strategies for defensible annual sums of net ecosystem exchange. Agric for Meteorol 107:43–69. https://doi.org/10.1016/S0168-1923(00)00225-2
Fang B, Lakshmi V, Jackson TJ et al (2019) Passive/active microwave soil moisture change disaggregation using SMAPVEX12 data. J Hydrol 574:1085–1098. https://doi.org/10.1016/j.jhydrol.2019.04.082
Fisher JB, Melton F, Middleton E et al (2017) The future of evapotranspiration: global requirements for ecosystem functioning, carbon and climate feedbacks, agricultural management, and water resources: the future of evapotranspiration. Water Resour Res 53:2618–2626. https://doi.org/10.1002/2016WR020175
Foster T, Gonçalves IZ, Campos I et al (2019) Assessing landscape scale heterogeneity in irrigation water use with remote sensing and in situ monitoring. Environ Res Lett 14:024004
Fratini G, Mauder M (2014) Towards a consistent eddy-covariance processing: an intercomparison of EddyPro and TK3. Atmos Measurement Techn 7:2273–2281
Gutman G, Ignatov A (1998) The derivation of the green vegetation fraction from NOAA/AVHRR data for use in numerical weather prediction models. Int J Remote Sens 19:1533–1543. https://doi.org/10.1080/014311698215333
Ha W, Gowda PH, Howell TA (2013) A review of downscaling methods for remote sensing-based irrigation management: part I. Irrig Sci 31:831–850. https://doi.org/10.1007/s00271-012-0331-7
Hartz TK (1996) Water management in drip-irrigated vegetable production. Horttech 6:165–167. https://doi.org/10.21273/HORTTECH.6.3.165
Jones JW, Hoogenboom G, Porter CH et al (2003) The DSSAT cropping system model. Eur J Agron 18:235–265
Kerr YH (2007) Soil moisture from space: where are we? Hydrogeol J 15:117–120. https://doi.org/10.1007/s10040-006-0095-3
Kljun N, Calanca P, Rotach MW, Schmid HP (2015) A simple two-dimensional parameterisation for flux footprint prediction (FFP). Geosci Model Dev 8:3695–3713. https://doi.org/10.5194/gmd-8-3695-2015
Kumar A, Chen F, Niyogi D et al (2011) Evaluation of a photosynthesis-based canopy resistance formulation in the Noah land-surface model. Boundary-Layer Meteorol 138:263–284. https://doi.org/10.1007/s10546-010-9559-z
Kumar SV, Peters-Lidard CD, Santanello JA et al (2015) Evaluating the utility of satellite soil moisture retrievals over irrigated areas and the ability of land data assimilation methods to correct for unmodeled processes. Hydrol Earth Syst Sci 19:4463–4478. https://doi.org/10.5194/hess-19-4463-2015
Kuslu Y, Dursun A, Sahin U et al (2008) Short communication. Effect of deficit irrigation on curly lettuce grown under semiarid conditions. Span J Agric Res 6:714. https://doi.org/10.5424/sjar/2008064-367
Leng G, Leung LR, Huang M (2017) Significant impacts of irrigation water sources and methods on modeling irrigation effects in the ACME L and Model. J Adv Model Earth Syst 9:1665–1683. https://doi.org/10.1002/2016MS000885
Liu X, Chen F, Barlage M, Niyogi D (2020) Implementing dynamic rooting depth for improved simulation of soil moisture and land surface feedbacks in Noah-MP-Crop. J Adv Model Earth Syst. https://doi.org/10.1029/2019MS001786
Malik W, Dechmi F (2019) DSSAT modelling for best irrigation management practices assessment under Mediterranean conditions. Agric Water Manage 216:27–43. https://doi.org/10.1016/j.agwat.2019.01.017
Massari C, Modanesi S, Dari J et al (2021) A review of irrigation information retrievals from space and their utility for users. Remote Sens 13:4112. https://doi.org/10.3390/rs13204112
McDonald MG, Harbaugh AW (1988) A modular three-dimensional finite-difference ground-water flow model. US Geological Survey, USA
Ozdogan M, Yang Y, Allez G, Cervantes C (2010) Remote sensing of irrigated agriculture: opportunities and challenges. Remote Sens 2:2274–2304. https://doi.org/10.3390/rs2092274
Peng J, Albergel C, Balenzano A et al (2021) A roadmap for high-resolution satellite soil moisture applications—confronting product characteristics with user requirements. Remote Sens Environ 252:112162. https://doi.org/10.1016/j.rse.2020.112162
Planet (2017) Planet application program interface: in space for life on earth. San Francisco, CA. 2017. https://api.planet.com
Raes D, Steduto P, Hsiao TC, Fereres E (2009) AquaCrop—the FAO crop model to simulate yield response to water: II. Main algorithms and software description. Agron J 101:438–447
Reichstein M, Falge E, Baldocchi D et al (2005) On the separation of net ecosystem exchange into assimilation and ecosystem respiration: review and improved algorithm. Glob Change Biol 11:1424–1439. https://doi.org/10.1111/j.1365-2486.2005.001002.x
Rosa R, Tanny J (2015) Surface renewal and eddy covariance measurements of sensible and latent heat fluxes of cotton during two growing seasons. Biosys Eng 136:149–161. https://doi.org/10.1016/j.biosystemseng.2015.05.012

Roux B, van der Laan M, Vahrmeijer T et al (2016) Estimating water footprints of vegetable crops: influence of growing season, solar radiation data and functional unit. Water 8:473. https://doi.org/10.3390/w8100473

Sanchez CA, Zerihun D, Farrell-Poe KL (2009) Management guidelines for efficient irrigation of vegetables using closed-end level furrows. Agric Water Manage 96:43–52. https://doi.org/10.1016/j.agwat.2008.06.010

Song Y, Jain AK, McIsaac GF (2013) Implementation of dynamic crop growth processes into a land surface model: evaluation of energy, water and carbon fluxes under corn and soybean rotation. Biogeosciences 10:8039–8066. https://doi.org/10.5194/bg-10-8039-2013

Taghvaeian S, Andales AA, Allen LN et al (2020) Irrigation scheduling for agriculture in the United States: The progress made and the path forward. Trans ASABE 63:1603–1618

Tasumi M (2019) Estimating evapotranspiration using METRIC model and Landsat data for better understandings of regional hydrology in the western Urmia Lake Basin. Agric Water Manage 226:105805. https://doi.org/10.1016/j.agwat.2019.105805

Thompson RB, Gallardo M, Valdez LC, Fernández MD (2007) Using plant water status to define threshold values for irrigation management of vegetable crops using soil moisture sensors. Agric Water Manage 88:147–158. https://doi.org/10.1016/j.agwat.2006.10.007

Thorup-Kristensen K (2001) Root growth and soil nitrogen depletion by onion, lettuce, early cabbage and carrot. Acta Hortic. https://doi.org/10.17660/ActaHortic.2001.563.25

Vickers D, Mahrt L (1997) Quality control and flux sampling problems for tower and aircraft data. J Atmos Ocean Technol 14:512–526

Webb EK, Pearman GI, Leuning R (1980) Correction of flux measurements for density effects due to heat and water vapour transfer. Q J R Meteorol Soc 106:85–100

Wieczorek M (2014) Area- and depth- weighted averages of selected SSURGO variables for the conterminous United States and District of Columbia. U.S. Geological Survey, Reston, VA

Williams JR (1995) The EPIC model. In: Singh VP (ed) Computer models of watershed hydrology. Water Reource Publication, USA, pp 909–1000

Xu C, Leskovar DI (2014) Growth, physiology and yield responses of cabbage to deficit irrigation. Hort Sci (prague) 41:138–146. https://doi.org/10.17221/208/2013-HORTSCI

Ye N, Walker JP, Guerschman J et al (2015) Standing water effect on soil moisture retrieval from L-band passive microwave observations. Remote Sens Environ 169:232–242. https://doi.org/10.1016/j.rse.2015.08.013

Yue J, Tian J, Tian Q et al (2019) Development of soil moisture indices from differences in water absorption between shortwave-infrared bands. ISPRS J Photogramm Remote Sens 154:216–230. https://doi.org/10.1016/j.isprsjprs.2019.06.012